A Study on Mechanism of Local Dot Positioning Errors Caused by a Paper Fed into Second Transfer

Takashi Hashimoto, Toshiyuki Andoh
Imaging Engine Development Division, Ricoh Co., Ltd.; Ebina, Kanagawa, Japan

Abstract

In a tandem printer, local dot positioning errors at a first transfer, which likely occur in thick paper printing, are unacceptable problems.

In this study, the mechanism of generating local dot positioning errors is investigated by FEM analysis. At first, vibration characteristics of a transfer belt drive system are investigated experimentally. And then, motion and deformation of a belt, a paper and rollers with the vibration characteristics are analyzed by FEM. Finally, calculated belt velocity fluctuation is validated by comparison with experiments.

As a result, it is clarified that the local dot positioning errors by belt velocity fluctuation at the first transfer are generated by belt tension and torque fluctuations on the drive shaft caused by impacts when leading edge of the thick paper is fed into a second transfer nip region. It has been known that the impacts generate a torque fluctuation on the drive shaft in a belt drive system as well as a steel rolling mill system. However, it is found in the result that they also generate a belt tension fluctuation in a pre-nip region caused by a contact force between a belt and a paper.

Present calculations can also provide image quality deterioration levels affected by jitter since the practical velocity fluctuations are accurately simulated.

Introduction

In a tandem printer, local dot positioning errors at a first transfer, which likely occur in thick paper printing, are unacceptable problems. As shown in Figure 1, they are caused by a transfer belt velocity fluctuation when leading edge of the thick paper is fed into a second transfer nip region. Therefore, it is necessary that the belt velocity fluctuation is calculated and mechanism of generating local dot positioning errors is investigated.

In recent years, slippage of transferred images caused by a velocity difference between an OPC drum and a paper has been studied [1]. Jitter caused by the vibration of a print-head carriage system has been studied [2]. Torque fluctuation on the drive shaft for a rolling mill has been calculated [3]. Drive torque when a thick paper goes into a roll nip has been calculated [4]. Mechanism of pinching belt conveyor [5] has been analyzed by FEM. However, FEM analysis with the vibration characteristics of a transfer belt drive system has not been studied yet.

In this study, vibration characteristics of a belt drive system are investigated experimentally. And then, motion and deformation of a belt, a paper and rollers with the vibration characteristics are analyzed by FEM. Finally, calculated belt velocity fluctuation is validated by comparison with experiments and mechanism of generating local dot positioning errors is investigated.

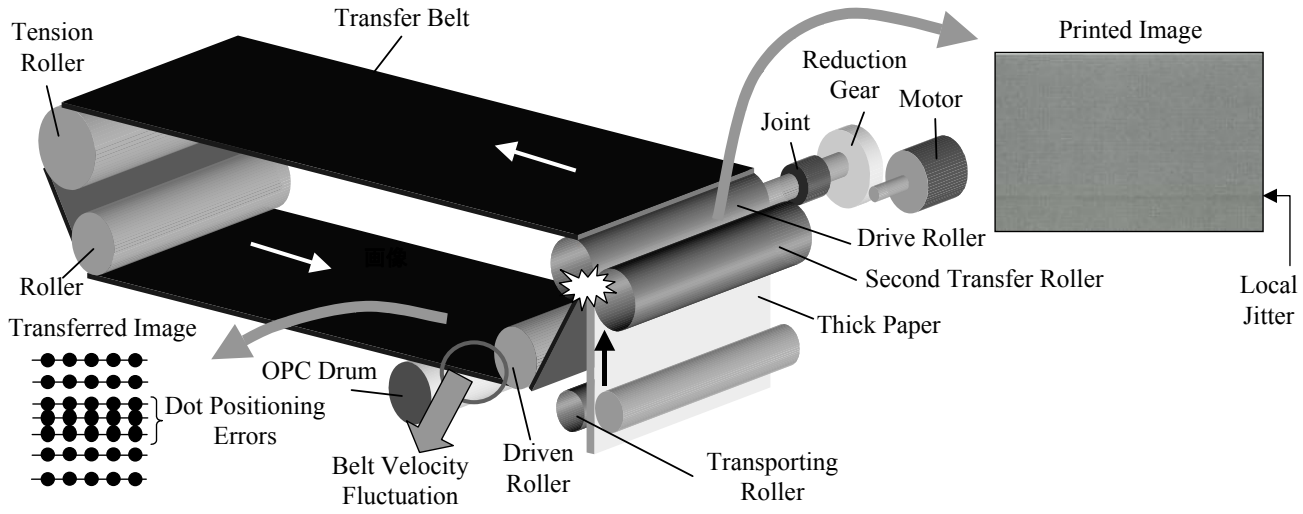

Figure 1. Schematic diagram of mechanism of generating local jitter

Vibration Characteristics of a Belt Drive System

Experimental Apparatus

As shown in Figure 1, a belt drive system consists of a transfer belt unit and a drive unit. A transfer belt is stretched over four rollers and pressed by a second transfer roller opposite to a drive roller. The transfer belt unit is jointed to the drive unit that consists of a DC motor and a reduction gear. A paper is fed into a second transfer nip by feed rollers. A rotary encoder is mounted on each shaft of a drive roller and a driven roller. Angular velocity and current of the motor are also measured in the apparatus. In this study, angular velocity of the driven roller is regarded as the belt velocity at a first transfer.

Frequency Response

Frequency response of a belt drive system was obtained using a swept-sine analysis with a dynamic signal analyzer. The system input is the voltage supplied to a PWM amplifier for applications using DC motor in current mode. Figure 2 (a) shows the frequency response from angular velocity of a drive roller to that of a driven roller. The phase is gradually lagging, however the magnitude is constant at nearly 0db from 10Hz to 150Hz. Therefore a transfer belt unit can be modeled as a 1-inertia system. Figure 2 (b) shows the frequency response from motor current to angular velocity of a drive roller. It indicates a resonant frequency at nearly 105Hz. Therefore a belt drive system can be modeled as a 2-inertia system that consists of a drive unit and a transfer belt unit.

Parameter Identification

Figure 3 shows block diagram of a belt drive system. It is necessary to identify the following unknown parameters in this system.

- Damping coefficient D_M of a drive unit
- Static load S_M of a drive unit
- Damping coefficient D_R of a transfer belt unit
- Static load S_R of a transfer belt unit
- Torsion stiffness k_S
- Torsion damping coefficient D_S

Damping coefficient D_M of the drive unit is obtained using a time constant T_a that is calculated from the step response of the drive unit. The input is motor current and the output is angular velocity of the motor. The transfer function between the input and output is given by

$$G_1(s) = \frac{K_a}{T_a s + 1},\ T_a = \frac{J_M}{D_M},\ K_a = \frac{K_e}{D_M}. \quad (1)$$

The step response between the input and output is given by

$$g(t) = K_a(1 - e^{-t/T_a}). \quad (2)$$

Therefore the time constant T_a is calculated from the experimental result using $g(\infty) = K_a$ and $g(T_a) = K_a(1 - 1/e)$.

Damping coefficient D_R of the transfer belt unit is obtained using a time constant T_b that is calculated from the step response of the belt drive system. The input is motor current, and the output is angular velocity of the driven roller. Modeled as a 1-inertia system where torsion stiffness is infinite, the transfer function between the input and output is given by

$$G_2(s) = \frac{K_b}{T_b s + 1},\quad T_b = \frac{n^2 J_M + J_R}{n^2 D_M + D_R},$$

$$K_b = \frac{K_e}{n^2 D_M + D_R}. \quad (3)$$

Therefore D_R can be obtained as well as D_M.

S_M and S_R are obtained using torque equilibrium equations as follows:

$$K_e i_M = D_M \omega_M + S_M,$$
$$K_e i_R = D_M(n\omega_R) + S_M + (D_R \omega_R + S_R)/n. \quad (4)$$

Torsion stiffness k_S is obtained using characteristic frequency of the 2-inertia system on the drive shaft as follows:

$$f = \frac{1}{2\pi}\sqrt{\frac{k_S s(n^2 J_M + J_R)}{n^2 J_M J_R}}. \quad (5)$$

Torsion damping coefficient D_S is obtained fitting calculated results to experiments of the frequency response at a resonant frequency.

Figure 4 shows calculated frequency response using the empirical model, which is compared to the experimental measurement. Both responses agree well, except the phase after a resonant frequency. The most probable reason of this result is due to damping non-linearity, which is not included in the 2-inertia system model. Thus, the vibration characteristics of a belt drive system are identified.

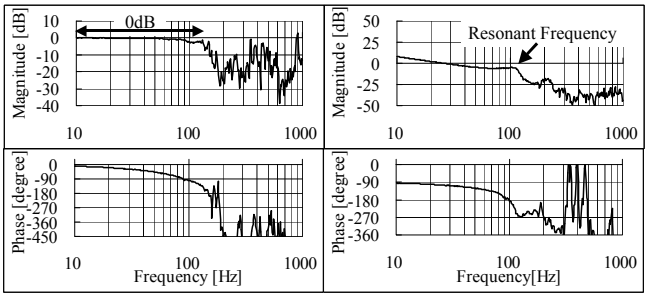

(a) From angular velocity of a drive roller to that of a driven roller

(b) From motor current to angular velocity of a drive roller

Figure 2. Frequency response of a belt drive system

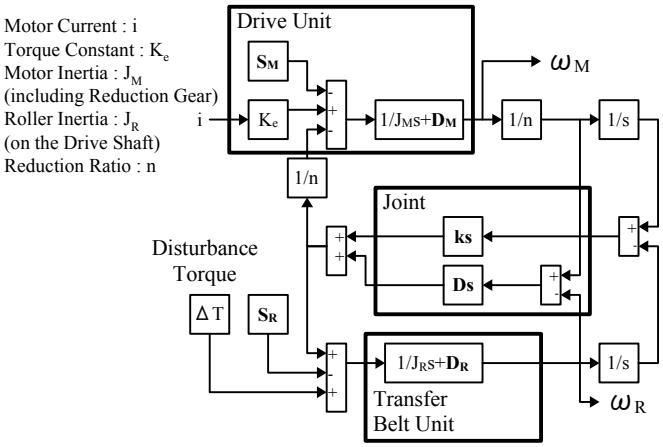

Figure 3. Block diagram of a belt drive system

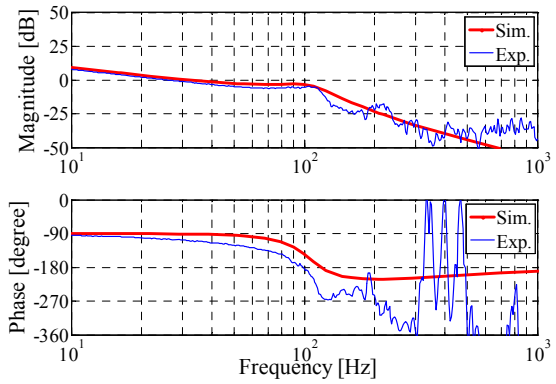

Figure 4 Comparison between calculated and experimental frequency response of a belt drive system

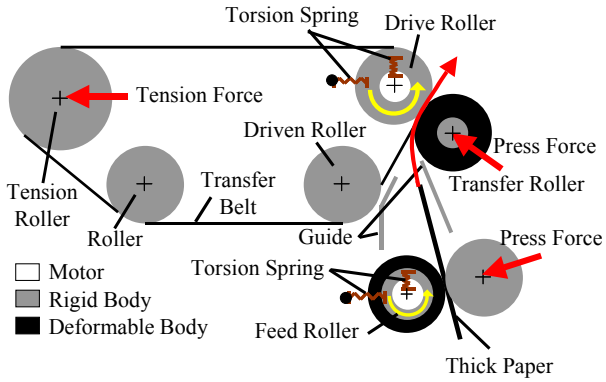

Figure 5. Simulation model

Finite Element Method

Simulation Model

Motion and deformation of a belt, a paper and rollers with the vibration characteristics are analyzed by FEM software Marc. Figure 5 shows a simulation model of the experimental apparatus. A belt, a paper, a second transfer roller and a feed roller are modeled as deformable body and meshed to quad elements of plain strain solid. The numbers of elements of each body are (7200, 2), (659, 3), (480, 12), and (240, 5), respectively. The others are modeled as rigid body. A drive roller is also modeled as rigid body because a rubber layer is enough thin to deform little. Main parameters of the simulation model are shown in Table 1.

The identified vibration characteristics are reflected in the simulation model. D_R and S_R are applied to damping coefficient and initial load of a torsion spring between the drive roller and an XY origin. D_S and k_S are applied to damping coefficient and stiffness of a torsion spring between the drive roller and the motor. D_M and S_M are not reflected because constant rotational displacement is given to the motor. The vibration characteristics in the feed roller system are also reflected, which are identified using a test bench.

The belt velocity fluctuation when leading edge of the thick paper is fed into a second transfer nip region is calculated using dynamic transient analysis.

Table 1. Main parameters of simulation model

Component	Thickness [μm]	E [MPa]	ν	μ
Belt	80	3000	0.42	-
Paper	250 (256 g/m^2)	6200	0.3	$\mu_{B\text{-}P}$=0.2
Transfer Roller	-	0.73	0.49	$\mu_{B\text{-}T}$=1, $\mu_{P\text{-}T}$=0.6
Feed Roller	-	8.3	0.49	$\mu_{P\text{-}F}$=1
Drive Roller	-	-	-	$\mu_{B\text{-}D}$=1.3
Other Rollers	-	-	-	$\mu_{B\text{-}O}$=0.1, $\mu_{P\text{-}O}$=0.1

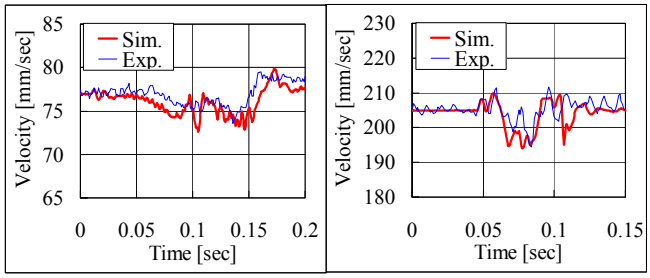

(a) Feed Velocity 77mm/sec (b) Feed Velocity 205mm/sec

Figure 6. Comparison between calculated and experimental angular velocities of the driven roller

Experimental Validation of Simulation Model

The calculated belt velocity fluctuation is validated by comparison with experiments. Figure 6 (a) and (b) show calculated and experimental angular velocities of the driven roller at feed velocity 77mm/sec and 205mm/sec. Both results agree well at each feed velocity, which supports the validity of the simulation model.

Mechanism of Generating Belt Velocity Fluctuation

Mechanism of generating belt velocity fluctuation is clarified with the simulation models for motion and deformation. Figure 7 shows snapshots of motion and deformation.

As shown in Figure 7 (a), angular velocity of the driven roller is increasing when leading edge of the thick paper is fed into a pre-nip region. Stretched belt between the drive and driven rollers is pushed inward by leading edge of the thick paper. Therefore the driven roller is subjected to accelerating torque and belt velocity is increasing. As shown in Figure 6 (a), angular velocity of the driven roller is increasing little at feed velocity 77mm/sec, which shows that as feed velocity is faster, angular velocity of the driven roller is more increasing.

As shown in Figure 7 (b), angular velocity of the driven roller is decreasing when leading edge of the thick paper is fed into a primary-nip region. The paper cannot be fed forward until a second transfer roller is pushed down to thickness of paper. In fact, additional torque of the drive roller is needed to push down the second transfer roller through the paper as well as a rolling mill system. Therefore the drive and driven rollers are subjected to reducing torque and belt velocity is decreasing.

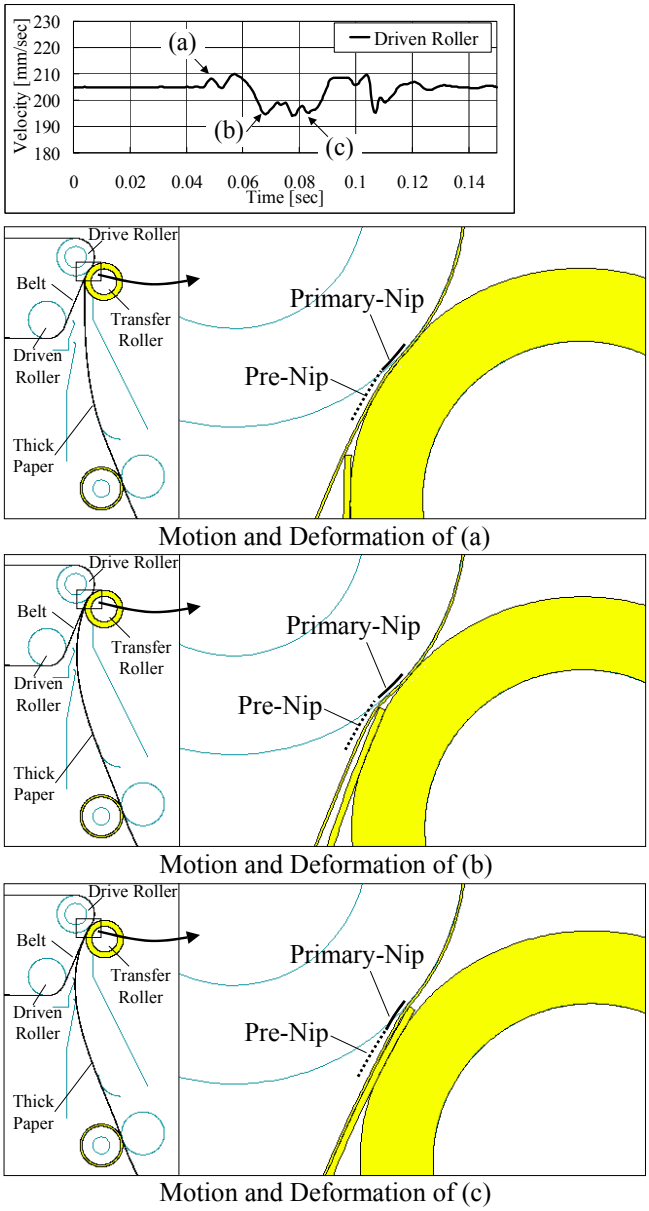

Figure 7. Snapshots of motion and deformation

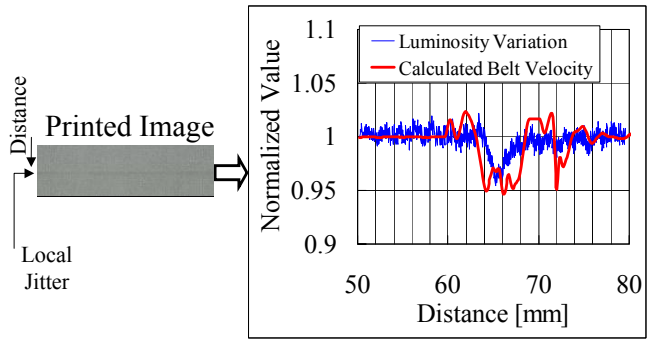

Figure 8. Comparison between calculated belt velocity and luminosity variation

As shown in Figure 7 (c), angular velocity of the driven roller is decreasing when the second transfer roller is pushed down to thickness of paper. Stretched belt between the drive and driven rollers pushed inward by the thick paper returns as its reaction. In fact, the opposite phenomenon from the snapshot shown in Figure 7 (a) occurs. Therefore the driven roller is subjected to reducing torque and belt velocity is decreasing.

Thus, the belt velocity fluctuation is generated by not only torque fluctuation on the drive shaft but also belt tension fluctuation in a pre-nip region when leading edge of the thick paper is fed into a second transfer nip region.

Comparison between Calculated Results and Printed Image

Figure 8 shows comparison between calculated belt velocity and luminosity variation for black halftones in thick paper printing. As shown in Figure 8, both results agree well, which enables the calculations to provide image quality deterioration levels affected by jitter.

Conclusion

In this study, vibration characteristics of a belt drive system are investigated experimentally. And then, belt velocity fluctuation when leading edge of the thick paper is fed into a second transfer nip region is calculated by FEM with vibration characteristics. Finally, calculated belt velocity fluctuation is validated by comparison with experiments. As a result, it is clarified that the belt velocity fluctuation is generated by not only torque fluctuation on the drive shaft but also belt tension fluctuation in a pre-nip region when leading edge of the thick paper is fed into a second transfer nip region. Present calculations can also provide image quality deterioration levels affected by jitter since the practical velocity fluctuations are accurately simulated.

References

[1] T. Nishigaito, K. Okuna and H. Ishi, “A Method for Analyzing Behavior to Prevent Slippage of Transferred Images in Laser Printers”, JSME. C, VOL. 60, NO. 557, pp. 3164-3170(1994)

[2] W. Zhang, K. Katano and T. Koyama, “A Study on Jitter of Serial Printer (Vibration Analysis of Carriage System)”, JSME. C, VOL. 67, NO. 664, pp. 3702-3707(2001)

[3] K. Yoshida and T. Osaka, “A Study on the Feeding Limit of Sheet Transporting Rollers”, JSME. C, VOL. 65, NO. 638, pp. 4129-4134(1999)

[4] A. Inoue, T. Nishida, M. Oda, T. Kikkawa and S. Takaoka, “Analysis of Torque Variation on the Drive Shaft for a Rolling Mill”, Dynamics & Design Conference, VOL. 1999, NO. A, pp. 363-366(1999)

[5] S. Yanabe, R. Shoji, D. Hayashi and C. Hui, “Traveling Distances of Belts and Medium in Pinching Belt Conveyor”, JSME. C, VOL. 74, NO. 742, pp. 1423-1431(2008).

Author Biography

Takashi Hashimoto received his ME in mechanical engineering from the University of Tokyo, Japan in 2004. He joined Ricoh in 2004 and has been engaged in R&D of printing technologies. He has focused on the development of simulation technologies for a belt drive system.